

Proceedings of the Fifth International Conference on
Railway Technology:
Research, Development and Maintenance
Edited by J. Pombo
Civil-Comp Conferences, Volume 1, Paper 21.14
Civil-Comp Press, Edinburgh, United Kingdom, 2022, doi: 10.4203/ccc.1.21.14
©Civil-Comp Ltd, Edinburgh, UK, 2022

Damage assessment in a wheel steel under dry-lubricated contact by an innovative vision system

**I. Bodini¹, A. Danesi¹, C. Petrogalli¹, A. Mazzù¹, T. Kato²,
and T. Makino²**

**¹Department of Mechanical and Industrial Engineering,
University of Brescia, Italy**

**²Steel Research Laboratory, Nippon Steel Corporation,
Amagasaki, Japan**

Abstract

The alternation of dry and wet contact can cause severe damage on railway wheels, because ratcheting occurring in dry contact leads to the formation of surface cracks, which can propagate if water is subsequently added, owing to the entrapped fluid pressurization mechanism. In a previous work, damage in alternated dry-wet contact was studied by means of twin-disc tests, aided by an innovative vision system including two devices: one for assessing the surface status by elaborating lights and shadows due to a diffused laser light projected on the specimen surface (2D analysis), the other for quantifying the local damage depth by elaborating the deformations of a projected laser blade (3D analysis). In that work, the 2D analysis resulted effective in revealing the onset of diffused fatigue crack propagation before it could be detected by vibration increment or visible spalling, but it failed when the damage was local; on the contrary, 3D analysis was effective in evaluating the damage severity only when the final failure had occurred.

In this paper, the 2D analysis method was improved, including localised analyses in addition to the analysis of the whole contact surface. Two tests were considered: one with alternated dry-wet contact sessions of 50000 cycles each, the other with a one million cycle dry session followed by wet contact up to failure. The 2D analysis results were compared with the 3D analysis ones; furthermore, at the end of the tests the specimens were cut at the locations where the vision systems indicated severe damage. In the test with short alternated dry-wet sessions the local 2D analysis results showed the same trend as the global ones: indeed, in this test the damage was diffused along

the specimen surface, the final failure resulting in many spalls all over the surface. Comparing the results of the 2D and 3D vision analyses with the observed crack depth, a general agreement was found.

In the test with the long dry contact session before the wet one, an agreement between the local 2D and 3D again was found only if the 2D analysis was performed locally, as the failure was determined by few large spalls. Again, a general agreement was found between the 2D analysis results and the observed subsurface crack depth.

The improvement of the 2D analysis procedure showed therefore the effectiveness of this method as an on-line non-destructive diagnostic tool even in case of localised damage.

Keywords: rolling contact fatigue, dry-wet contact, assessment, vision-based analysis.

1 Introduction

The alternation of dry and wet contact can cause severe damage on railway wheels. Indeed, in dry contact, the high frictional forces induce ratcheting below the contact surface, up to the formation of inclined surface cracks. Wear mitigates crack propagation by removing material layers from the surface, this way stabilizing the depth of the surface cracks [1,2]. However, if water is subsequently added to such a deteriorated surface, surface cracks can propagate, owing to the fluid entrapped inside the cracks that is pressurized at each load passage [3,4].

Bodini et al. [5,6] studied the effect of alternated dry and wet contact by means of twin-disc tests, aided by an innovative vision system used for analyzing the contact surface[7]. In particular, such system includes two distinct devices: one for evaluating the damage by analyzing lights and shadows on images obtained by scanning the contact surface along the tangential direction (named 2D analysis); the other one for reconstructing the radial profile of the contact surface by analyzing the deformation of a laser blade projected on the contact surface (named 3D analysis). They found that the duration of the alternated dry-wet contact sessions has a strong influence on the specimen life: short sessions have a beneficial effect, because the surface crack formation by ratcheting, in the dry phases, is delayed by the occurrence of wet contact sessions with low friction. On the contrary, long dry-wet sessions accelerate the failure, because, in the dry session, surface cracks have more time to nucleate and, in wet sessions, more time to propagate. Furthermore, they found that the 2D analysis could reveal the beginning of fatigue crack propagation before it could be detected by appreciable vibration increment or visible spalling. However, once spalling occurred, a direct correlation between the 2D analysis damage parameters and the effective damage could not be found, as spalling was mainly a localized severe phenomenon, whereas the 2D analysis was averaged over the whole contact surface. Only the ex-post 3D analysis allowed evaluating the local damage severity.

In this paper, the 2D analysis was carried out locally, by averaging the damage parameters over limited portions of the contact surface, this way obtaining local damage parameters. The local 2D analysis was compared with the 3D analysis and with the subsurface damage evaluation obtained by destructive analysis, in order to

validate its capability of providing reliable information even about the severity of the spalling.

2 Methods

Rolling-sliding tests in dry and wet contact were carried out by means of a bi-disc test bench described in [5], and test conditions are presented in Table1:

Material	0.7%C steel with fine pearlite structure
Hardness	HV330
Maximum contact pressure	0.9 GPa
Rolling Speed	500 rpm
sliding/rolling ratio	0.5%
Lubricant (wet contact)	water with the addition of 10% glycol

Table1: Test conditions.

In this paper two tests are presented, called K4 and K8, as in Table2.

Test	Dry-wet sequence
K4	50k dry +50k wet+ ... + up to failure
K8	1.000.000 dry + n wet up to failure

Table2: Test conditions.

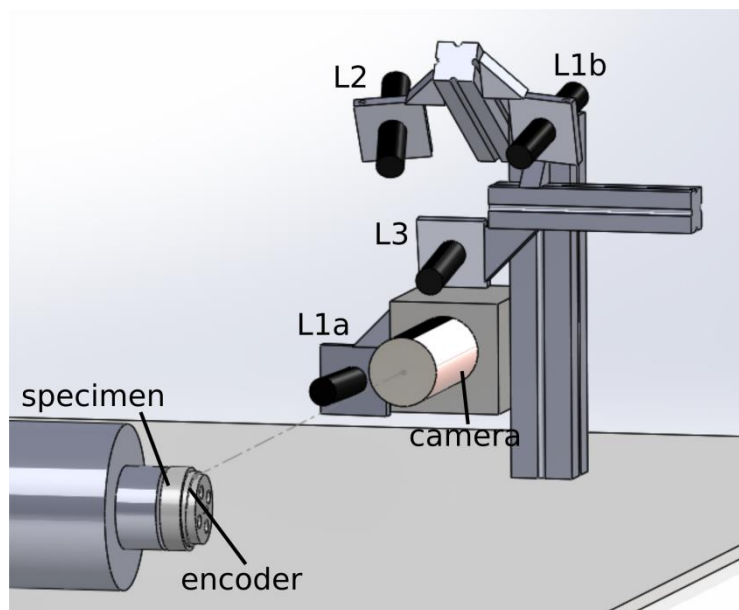


Figure 1: Scheme of the vision-based measurement system: high-speed camera C, defocused laser pointers L1a and L1b, laser stripes L2 and L3

Figure 1 shows a scheme of the vision-based measurement system mounted on the bi-disc test bench and described in [7].

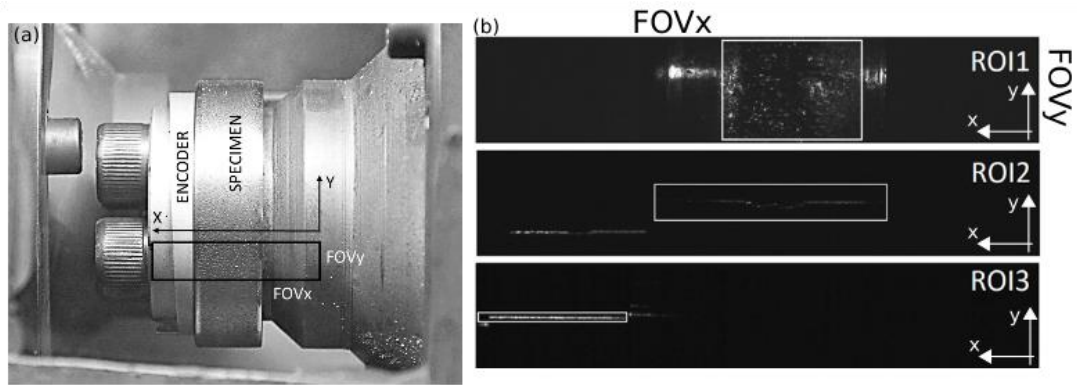


Figure 2: (a) Specimen and encoder mounted on the bi-disc test bench, and Field of View (FOV) of the camera. (b) FOV and Regions of Interest (ROIs) for image processing.

Figure 2(a) shows the Field of view (FOV) of 24 mm x 6 mm. Figure 2(b) shows the FOV acquired by the camera at a speed of 377 fps, and the defined regions of interest (ROI) which undergo different image processing [7], described in Table 3.

ROI	Figure	Image processing
ROI1 (a)	<p>Figure 2(b) ROI1 (a) and (b) showing the ROI1 region of interest.</p>	Threshold (b) + blob analysis to calculate R_B (damage ratio = the ratio between the sum of the areas of all the blobs in a ROI and the total area of the ROI)
ROI2 (c)	<p>Figure 2(b) ROI2 (c), (d), and (e) showing the ROI2 region of interest and its processing results.</p>	Threshold + centers of mass of the grey levels (d); measure (e)

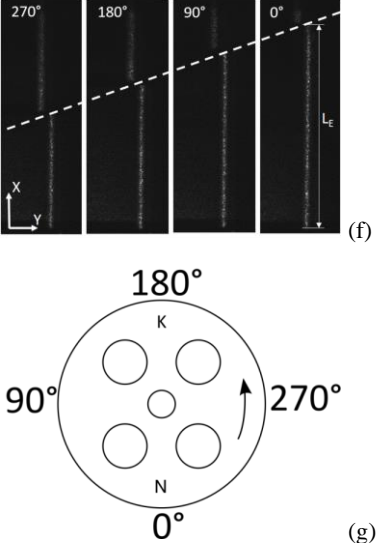
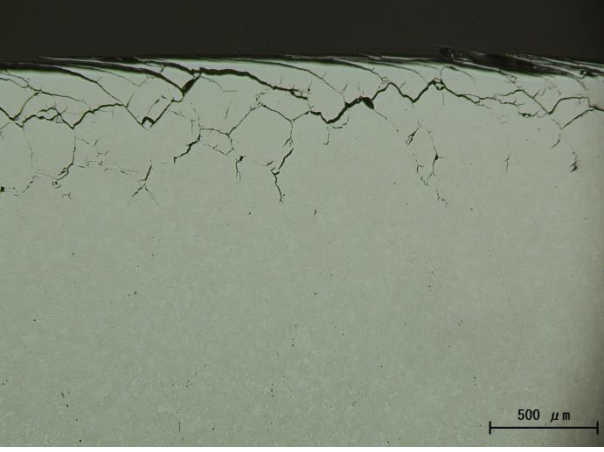
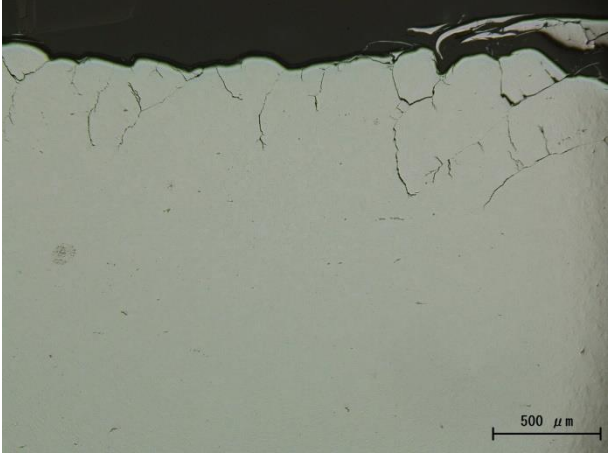
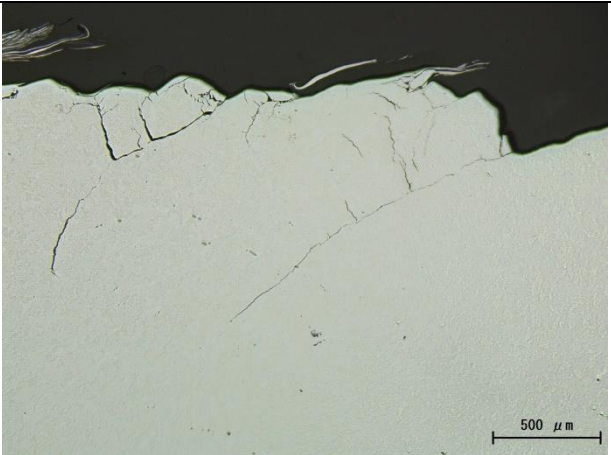
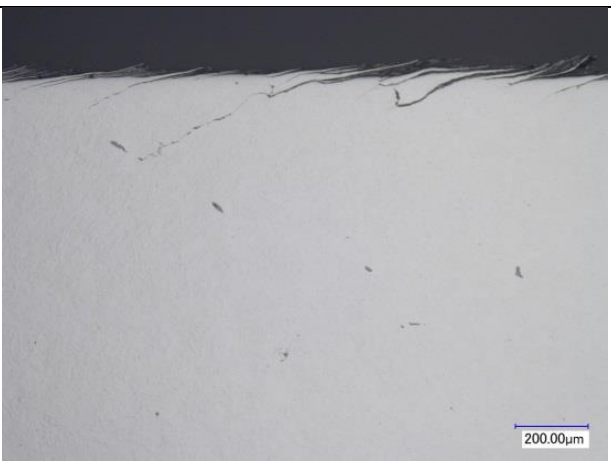
ROI3		<p>Threshold + centers of mass of the grey level + length L_E (f) calculation and correlation with the angular position of the portion of the specimen (g).</p>
------	---	--

Table3: Description of the image processing in each Region Of Interest.

In previous works [5,6], R_B has been calculated as average value over the entire specimen surface. In this work, some positions on the specimen surface have been chosen, after specimen failure, considering the measured 3D profiles, and the R_B histories have been reconstructed in these positions. Moreover, the specimens were cut in these positions and the crack depths have been measured.

3 Results

Specimen	Position [degrees]		
K8	17°		(a)

K8	103°		(b)
K8	290°		(c)
K4	295°		(d)

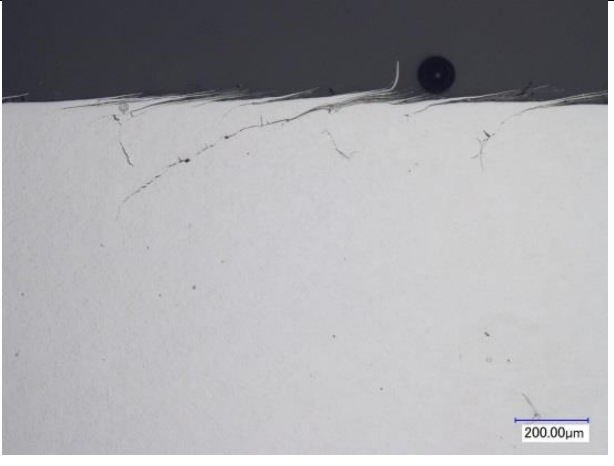
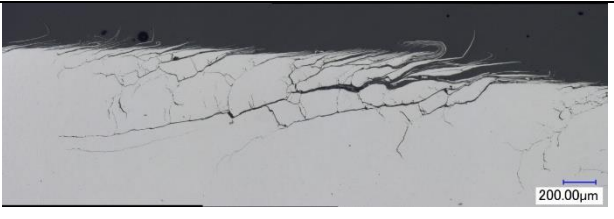
K4	320°		(e)
K4	240°		(f)

Table 4: Micrographs of specimen K8 and K4 in some defined position.

3D measurements were useful to choose the angular positions. Table 4 shows how the cracks are localized in the specimen, and how crack depth is not uniform when a specimen fails after alternating dry ad lubricated phases. Figure 7 shows the crack depth measurements in different angular positions for specimen K4 (Figure 7(a)) and for specimen K8 (Figure 7(b)). In particular, K4 maximum crack depth is located at 240 degrees, and K8 maximum crack depth is located at 290 degrees.

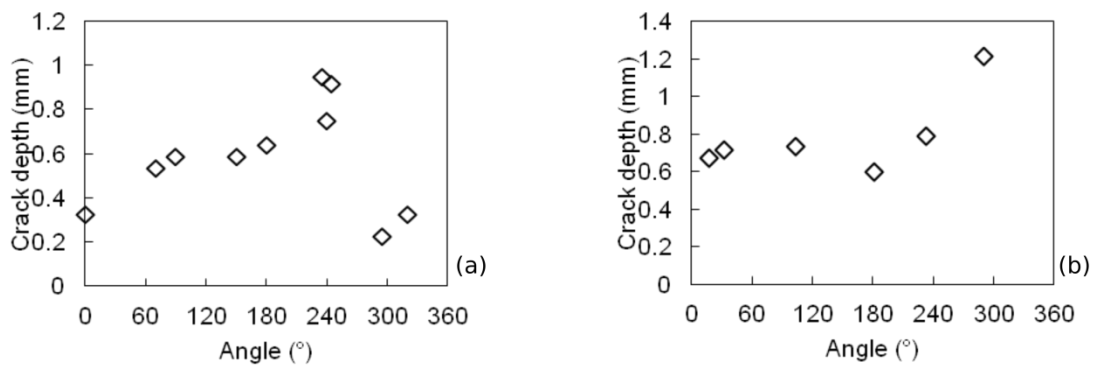


Figure 7: (a) K4 crack depths; (b) K8 crack depths.

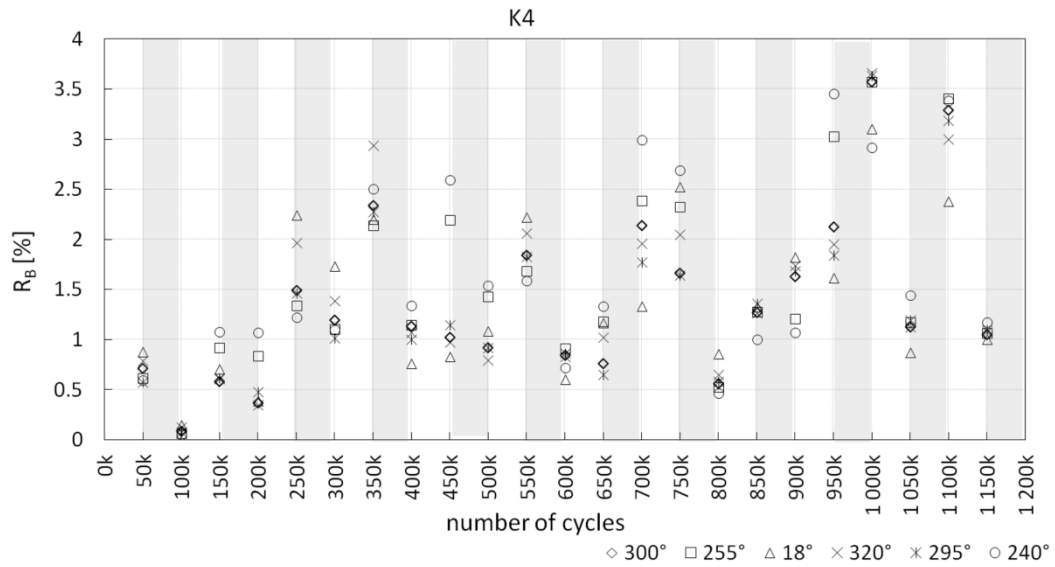


Figure 8: R_B histories in different angular position, for specimen K4.

Figure 8 shows the R_B evolution of the surface of the K4 specimen in defined angular positions, detected after failure. The white columns are dry phases and the grey columns are wet phases. The considered portions have similar damage ratio level, probably because K4 underwent alternated dry-lubricated phases, 50 kcycles each, and wear, which dominates in dry phases [5,6], probably mitigates the effects of fatigue. However, the portion presenting the longest crack depth (240 degrees, Figure 7(a)) is the one (the round symbol in Figure 8) which presents the higher values of R_B , during the whole life of the specimen.

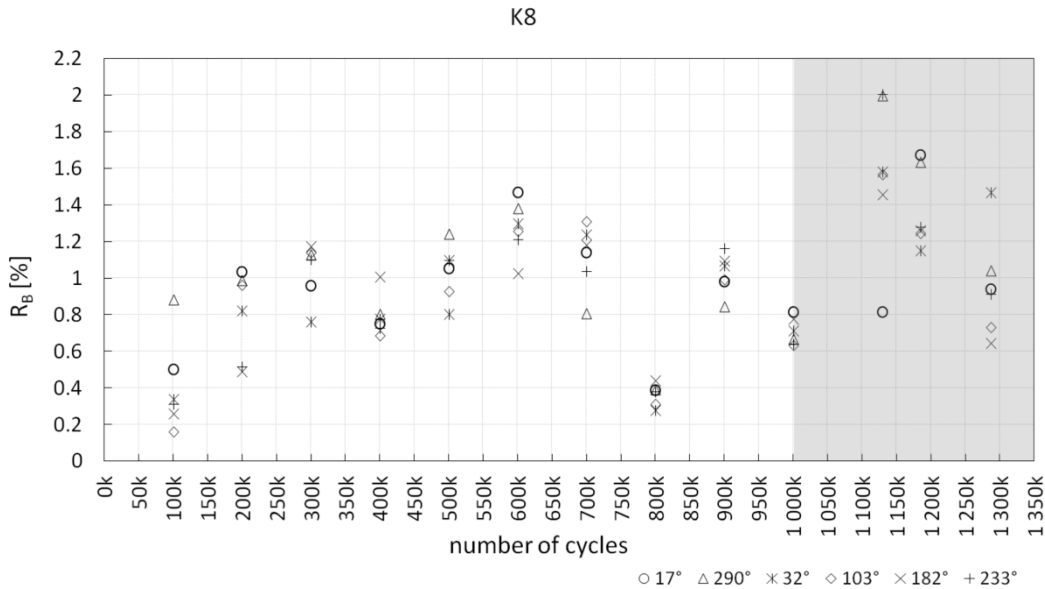
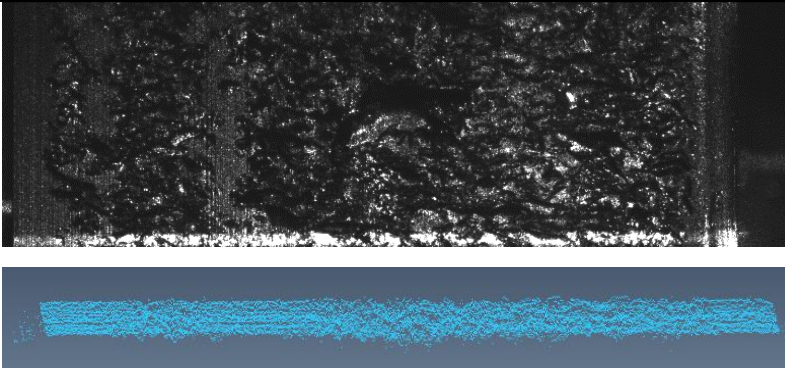
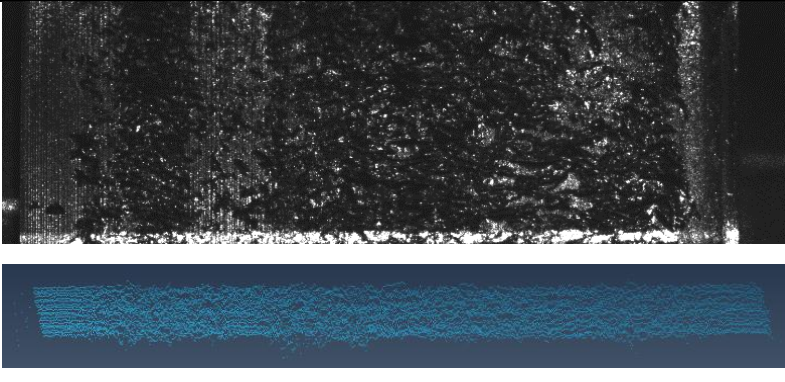
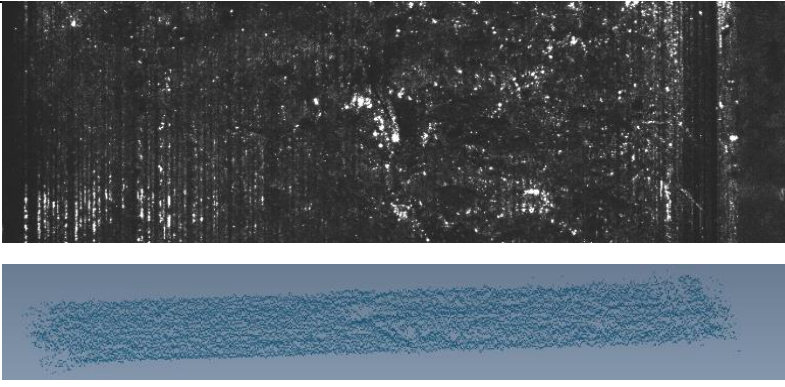


Figure 9: R_B histories in different angular position, for specimen K8.

Figure 9 shows the R_B evolution of the surface of the K8 specimen in defined angular positions, detected after failure. The white area is the dry phase, the grey area

is the lubricated phase. R_B is uniform in the whole dry phase; then, when lubricated phase starts, the damage appears different in different portions of the specimen. Observing both Figure 7(b) and Figure 9, it can be noted that the portion with the longest crack depth (290 degrees, Figure 7(b)) is the most damaged one when the lubricated phase starts (triangle symbol in Figure 9), and fatigue starts dominating.

Specimen	Position [degree]	2D image and corresponding 3D Point Cloud
K4	320°	
K4	240°	
K8	17°	

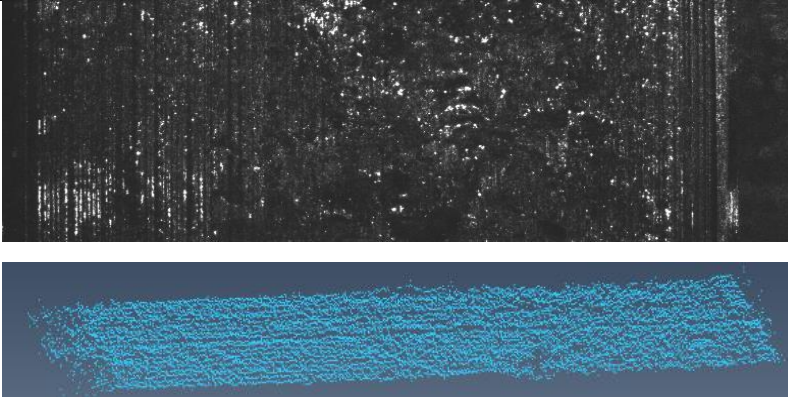
K8	290°	
----	------	--

Table5. Point cloud of portion of specimens in different angular positions.

The on-line 3D measurements were useful also to reconstruct the specimen surface after failure, as shown in Table 5.

4 Conclusions and Contributions

2D analysis was carried out locally, by averaging the damage parameters over limited portions of the contact surface, this way obtaining local damage parameters. The local 2D analysis was compared with the 3D analysis and with the subsurface damage evaluation obtained by destructive analysis, in order to validate its capability of providing reliable information even about the severity of the spalling. Analyzing the results it seems that the damage ratio R_B , locally calculated is representative of the damage level of the portion of the specimen and is useful to localize damaged areas on the specimen surface.

When wear is the dominating phenomenon, the portions of the specimens are uniformly damaged, and a localized analysis of R_B is not needed, therefore, R_B can be calculated as an average value over the whole specimen surface. When dry and lubricated phases are alternated, the damage of the specimens is not uniformly distributed on the surface, but it is localized. Calculating R_B locally could be useful when dry and wet phases are alternated and when there is competition between wear and fatigue effects, because it allows detecting damaged portions and to follow their evolution during tests.

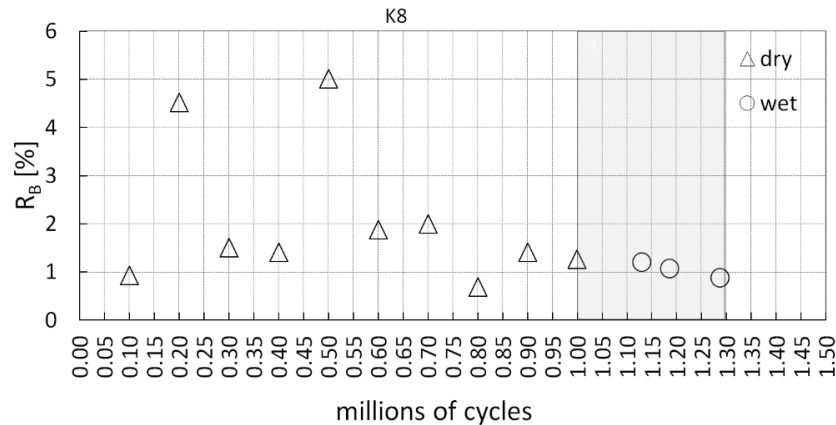


Figure 12: Average damage ratio R_B evolution of K8 specimen.

Figure 12 shows the evolution of average R_B of K8 specimen. When lubricated phase starts, the average R_B index does not significantly vary, as it does in Figure 10. Therefore, analyzing R_B index locally, a more accurate and significant evaluation of the specimen damage could be performed.

Further study will be performed to study possible correlation between R_B locally calculated during the tests, 3D damage measurements after failure, and crack depth after failure, calculated in the same detected positions.

References

- [1] M. Faccoli, et. al., "Rolling Contact Fatigue and Wear Behavior of High-Performance Railway Wheel Steels Under Various Rolling-Sliding Contact Conditions", *Journal of Materials Engineering and Performance*, 26(7), 3271-3284, 2017.
- [2] A. Mazzù, G. Donzella, "A Model for Predicting Plastic Strain and Surface Cracks at Steady-State Wear and Ratcheting Regime", *Wear*, 400, 127-136, 2018.
- [3] S. Maya-Johnson, J.F. Santa, A. Toro, "Dry and Lubricated Wear of Rail Steel under Rolling Contact Fatigue - Wear Mechanisms and Crack Growth", *Wear*, 380-381, 240-250, 2017.
- [4] T. Makino, T. Kato, K. Hirakawa, "The Effect of Slip Ratio on The Rolling Contact Fatigue Property of Railway Wheel Steel", *International Journal of Fatigue*, 36(1), 68-79, 2012.
- [5] I. Bodini, et. al., "Evaluation of Wear in Rolling Contact Tests by Means of 2D Image Analysis", *Wear*, 400, 156-168, 2018.
- [6] I. Bodini, et. al., "A Study of Wear and Rolling Contact Fatigue on a Wheel Steel in Alternated Dry-Wet Contact Aided by Innovative Measurement Systems", in F. Iacoviello, L. Susmel, D. Firrao, G. Ferro, (Editors), "Proceedings of the 25th International Conference on Fracture and Structural Integrity", *Procedia Structural Integrity*, 18, 849-857, 2019. doi:10.1016/j.prostr.2019.08.235

- [7] I. Bordini, et. al., “A novel optical apparatus for the study of rolling contact wear/fatigue based on a high-speed camera and multiple-source laser illumination”, *Review of Scientific Instruments* 87, 083701, 2016